COBEM 2023 27TH INTERNATIONAL CONGRESS OF MECHANICAL ENGENEERING

ABCM Brazilian Society of Mechanical Sciences and Engineering
27th ABCM International Congress of Mechanical Engineering
December 04-08, 2023, Florianópolis-SC, Brazil

COB-2023-0135
TRANSIENT THERMAL-ELECTRICAL MODEL FOR SIMULATING A PHOTOVOLTAIC MODULE
27th COBEM

Thaís de Vasconcelos Silva
Fabiano Cordeiro Cavalcanti
Instituiton: Renewable and Alternative Energy Center (CEAR) in Federal University of Paraíba (UFPB)
Adress: Cidade Universitária - João Pessoa - PB - Brasil - CEP: 58051-970
thaisvasconcelos@cear.ufpb.br, fabianofr@cear.ufpb.br

Cristiane Kelly Ferreira da Silva
Instituiton: Renewable and Alternative Energy Center (CEAR) in Federal University of Paraíba (UFPB)
Adress: Cidade Universitária - João Pessoa - PB - Brasil - CEP: 58051-970
cristianek@cear.ufpb.br

Gilberto Augusto Amado Moreira
Instituiton: Renewable and Alternative Energy Center (CEAR) in Federal University of Paraíba (UFPB)
Adress: Cidade Universitária - João Pessoa - PB - Brasil - CEP: 58051-970
gilberto@cear.ufpb.br

Abstract. *The exploitation of renewable energy sources has proven to be a viable solution for society in reducing its dependence on fossil fuels. As a consequence, the use of photovoltaic modules has grown strongly in recent years. It is known that the efficiency of converting solar energy into electricity in silicon-based photovoltaic modules can be affected by various factors, with the operating temperature of the photovoltaic cell being one of the most important. This work aims to develop a transient thermal-electric model of a photovoltaic module that enables the simulation of different modules under different operating conditions. The proposed modeling is based on a multi-physics perspective, which considers both the thermal and electrical phenomena involved in the photovoltaic generation of electricity. The adopted thermal model is one-dimensional and in transient heat transfer regime. It considers heat conduction through the thicknesses of the different layers of the materials that make up the module, thermal generation in the photovoltaic cells and glass, and radiative and convective heat exchanges that occur on the upper and lower surfaces of the module. Its numerical solution occurs via the finite difference method, with an implicit time scheme. The electrical model is based on a circuit composed of a practical diode, with a series resistance and another parallel one representing, respectively, the leakage current and the structural losses of the photovoltaic module. The solution of the transient thermal model is coupled with the electrical model, constituting the thermal-electrical model. The coupling between the two models occurs through a computational algorithm performed in MATLAB software. From the resolution of the transient thermal-electric model proposed in this work, the temperatures of the photovoltaic cell were calculated over simulated days. These results are compared to those calculated via other models available in the literature. In fact, if faced with an essentially thermal model of a photovoltaic module, the proposed thermal-electric model has the advantage of taking into account both the thermophysical and geometric parameters of the module as well as its electrical characteristics.*

Keywords: *photovoltaic module, thermal model, electrical model, photovoltaic efficiency.*

1. INTRODUCTION

Renewable energy sources will be the main ally in order to reduce the use of fossil fuels in the future, because of their clean and renewable characteristics. Solar energy applications can be classified in two main categories: solar thermal systems, that use solar energy for thermal applications, and photovoltaic systems, that convert solar energy directly into electrical power. According to IEA (2022), solar photovoltaic energy grew into 22% in the year if 2021, accounting for 3,6% of all electricity generated in the world.

The implementation of experimental studies with solar photovoltaic modules is costly and sometimes impractical. Therefore, the implementation of a computational model that is able to simulate the behavior of those systems become essential (Jakhrani, 2013).

Photovoltaic modules models have two main parameters: the electrical efficiency (η) and the cell temperature (T_{cel}). Such parameters are interdependent. In that sense, to accurately describe the behavior of a photovoltaic module, it is necessary to compute both thermal and electrical parameters (Tuza e Mahieddine, 2014).

Through literature review, different models were studied, such as the purely thermal models of Ross (1976), Mondol *et al.* (2005), Risser and Fuentes (1984), the thermal-electrical model of King *et al.* (2004) and an adaptation of Duffie *et al*. (2020). In the work of Ross (1976), the temperature of the photovoltaic cell is described as being proportional to solar irradiance. Risser and Fuentes (1984) collected data from four different photovoltaic modules and generated equations to estimate the cell temperature and generated power through linear regression, and their results indicate that those parameters are determined as functions of the climatic conditions. Mondol *et al.* (2005) developed a linear correlation which relates the temperature difference between module and ambient to insolation. King *et al.* (2004) developed an empirical thermal-electrical model based in data that was collected over twelve years and were tested in different laboratories. Through regression analysis, seven coefficients were calculated in order to estimate the thermal and electrical parameters of photovoltaic modules. Duffie *et al.* (2020) presents equations to predict the cell temperature and electrical parameters of the photovoltaic module. Through the coupling of those equations, a thermal-electrical model was adapted for comparison purposes and those results are further discussed in Section 3.

The implementation of a thermal-electrical model was opted for describing the behavior of the photovoltaic module. With this approach, both thermal and geometrical properties of the module are accounted for, as well as its electrical characteristics. Regarding the thermal segment of the modelling, the adopted hypothesis was that the module was a flat-plate of longitudinal uniform temperature in a transient heat transfer regime. It was considered that the temperature varies only along the module's thickness, composed by five layers of different materials. According to Brano *et al*. (2014), the simplification of the thermal model coming from the hypothesis of a unidimensional heat flux is justifiable, because the ratio between the thickness of the photovoltaic module and its surface area tends to be small. The electrical modelling developed was based on Villalva *et al* (2009).

The developed model was applied in simulated days and compared with other models found in literature, them being purely thermal and thermal-electrical. Graphs were plotted with data from variations of the photovoltaic cells' temperature (T_{cel}, in K) and electrical efficiency (η, dimensionless) of the module throughout the average days of March, June, September and December. The climatological data used as entry variables in the simulations correspond to the geographic location of the Center of Renewable and Alternative Energy (CEAR), located at the Federal University of Paraíba (UFPB), in João Pessoa, Brazil. The results will be discussed in Section 3 of this paper.

2. MATHEMATICAL MODELLING

The execution of the thermal-electrical model of the photovoltaic module is divided in two parts, the thermal modelling and the electrical modelling. This section describes each of these models and their coupling, aiming to obtain a thermal-electrical model. Before, it is described how the solar irradiance is calculated from the use of average irradiation data obtained in climatological databases, like NASA (2021).

2.1 Climatological Model

The climatological data used in the thermal-electrical model include the following parameters: the average wind speed (V_w, in m/s), the surface albedo (ρ_g, dimensionless) and the monthly average daily total irradiation on a horizontal surface ($\overline{H}$, em kWh/m²/day), the monthly average daily diffuse irradiation on the horizontal surface ($\overline{H}_d$, in kWh/m²/day) and the average air temperature (T_∞, in K). The selected simulation location was the Center of Renewable and Alternative Energy (CEAR), located at the Federal University of Paraíba, in João Pessoa, Brazil, with latitude $\phi = -7.14°$ and longitude l = -34.5º. The photovoltaic module in question was considered to be at an angle of $\beta_i =$ 10º in relation to the horizontal plane, and its collecting face oriented to the geographic north.

The average monthly values of the total solar irradiation and diffuse irradiation are converted into total irradiance and diffuse irradiance via an adaptation of the methodology described in Duffie and Beckmann (2020). Equation 1 provides the total solar irradiance (in W/m²) onto the tilted surface of the photovoltaic module.

$$G_i = R_b G_b + G_d \left(1 + \frac{\cos\beta_i}{2}\right) + G\rho_g \left(1 - \frac{\cos\beta_i}{2}\right) \quad (1)$$

where R_b is the ratio between beam solar irradiance on the tilted module ($G_{b,T}$ em W/m²) with relation to the beam irradiance on the horizontal plane (G_b, in W/m²) and G (in W/m²) is the total solar irradiation over the horizontal plane.

2.2 Electrical Model

The electrical model was developed from the analysis of the circuit present in Figure 1. Said circuit represents the equivalent circuit of the ideal photovoltaic cell e requires the knowledge of five parameters, which are: the photogenerated current (I_{pv}, em A), represented by a current source; the diode reverse saturation current (I_d, em A), that is composed by the reverse saturation current (I_0, em A); the series resistance (R_s, em Ω), originated by the sum of

various structural device resistances; the parallel resistance (R_p, em Ω), representing the losses due to leakage in the *p-n* junction and depends on the used manufacturing method. In addition, it is necessary to calculate the diode ideality factor a, that is related to the physical constants and the *n* parameter, known as ideality factor that has its value equal to 1 for an ideal diode and typically $1 \leq n \leq 2$ for real diodes (Villalva *et al.,* 2009.)

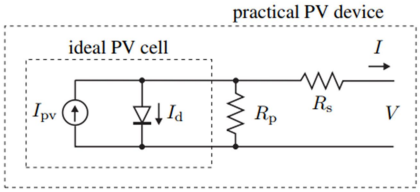

Figure 1. Single diode model of the theoretical photovoltaic cell and the equivalent circuit of the practical photovoltaic device.

The system described above can be represented by Equation 2 (Villalva *et al.,* 2009).

$$I = I_{pv} - I_0 \left[\exp\left(\frac{V + R_s I}{V_t a}\right) - 1\right] - \frac{V + R_s I}{R_p} \tag{2}$$

The developed electrical model is based on Villalva *et al* (2009). For the calculations of voltage (V, in V) and current (I, in A), the five unknown parameters of Eq. (2) must be determined: I_{pv}, I_0, R_s, R_p and a. The reverse saturation current (I_0, in A), the photogenerated current (I_{pv}, in A) and the diode ideality factor constant (a, dimensionless) are functions of R_s and R_p, both values given in Ω. To calculate the resistances, an iterative method is needed, in which R_p is calculated for R_s values between $0 < R_s < R_{s,max}$, until a pair $\{R_s, R_p\}$ results in the equality between the maximum power calculated by the model ($P_{max,m}$, in W) and the maximum experimental power provided in the photovoltaic module datasheet ($P_{max,e}$, in W). Both parameters are obtained at the maximum power point, where $P_{max,m} = V_{mp} I_{mp}$ (Villalva *et al.,* 2009). Therefore, the electrical efficiency η of the photovoltaic module can be calculated with Eq. (3),

$$\eta = \frac{P_{max,m}}{G_i \cdot \left(A_{PV,panel}\right)} \tag{3}$$

where $A_{PV,panel}$ is the frontal area of the photovoltaic module, in m².

After the calculations of R_s and R_p for the STC conditions (Standard Test Conditions), it is possible to calculate the electrical efficiency of the photovoltaic module for other conditions beyond STC, utilizing the previously found values of R_s and R_p. The parameter V in Eq. (2) is found between $0 < V < V_{oc}$, where V_{oc} (in V) is the open circuit voltage. A numerical method is needed to find a $\{V, I\}$ pair that results in the maximum electrical power produced by the photovoltaic module ($P_{max,m}$, in W).

2.3 Thermal Model

For the thermal model, a unidimensional heat transfer regime was adopted for the interior of the different layers of the materials that compose the photovoltaic module. The adopted direction was the transverse to the surface area of the module. The transient solution of the model was achieved via an implicit time discretization (Özişik, 2017). In Figure 2, the temperature of interest for the thermal-electrical model is the photovoltaic cell temperature, T_{cel} (in K). To calculate this temperature, an energy balance was applied in the control volumes, accounting the energy gain through incident radiation, G_i, on the module's upper glass layer, calculate by Eq. (1), and the portion of solar irradiation that is absorbed in the photovoltaic cells, S (in W/m²), given by Eq. (4), in accordance to Aly *et al.,* (2017).

$$S = \left(\tau_g \tilde{\alpha}_{PV}\right)_n \left[R_b G_b K_b + G_d K_d \left(\frac{1 + \cos\beta}{2}\right) + (G_b + G_d)\rho_{gr} K_{gr} \left(\frac{1 - \cos\beta}{2}\right)\right] \tag{4}$$

where $\tau_g \tilde{\alpha}_{PV}$ (dimensionless) is the product between the glass' transmittance and the photovoltaic cell absorptivity for solar irradiation. The dimensionless parameters K_b, K_d e K_g are the incident angle modifiers of direct, diffuse, and ground-reflected irradiance.

In this paper, the internal heat generation due to solar radiation absorption occurs only in the photovoltaic cell and glass domains. It was also considered that the layers of EVA and Tedlar do not have heat generation.

The generated heat within the photovoltaic cell ($\dot{Q}_{PV}$, in W/m³) is given by Eq. (5), according to Aly *et al* (2017).

$$\dot{Q}_{PV} = \frac{S \cdot A_{PV,cells} \cdot (1-\eta)}{V_{PV,cells}} \tag{5}$$

where $A_{PV,cells}$ (in m²) is the frontal surface area of the photovoltaic cells, $V_{PV,cells}$ (in m³) is the total volume of the cells and η is the module's electrical efficiency, determined through the solution of the previously presented electrical model.

The heat generated within the glass layer of the photovoltaic module ($\dot{Q}_G$, in W/m³) is given by Eq. (6), according to Aly *et al* (2017).

$$\dot{Q}_G = \frac{\alpha_g \cdot G_i \cdot A_{PV,panel}}{V_g} \tag{6}$$

where V_g (in m³) is the volume of the glass and α_g is the absorptivity of the glass to solar radiation.

The energy balance also accounts for the convective energy losses to ambient air above and below the photovoltaic module – assumed to be at the same temperature (T_∞, in K) – the radiative losses of the superior glass surface of the module to surrounding sink ($T_{glass-sk}$, $T_{glass-ground}$, in K) and the radiative heat losses from the inferior surface of the module's Tedlar to surrounding sink ($T_{tedlar-sky}$, $T_{tedla\quad ground}$, in K). The converted solar irradiance into electrical power (P_η, in W/m²) in the photovoltaic cells is indicated in Figure 2.

According to Incropera *et al* (2017), the heat losses are represented by their equivalent resistances. $R_{conv,f/b}$ (in m².K/W) represents the equivalent resistance due to convective heat transfer in the front surface of the upper glass layer or the back Tedlar with the sink. $R_{front,sky}$ and $R_{front,ground}$ are the equivalent resistances due to radiative heat transfer in the glass surface to the sky and to the ground. $R_{cond,f/b}$ are the equivalent resistances due to conductive heat transfer of the upper cell surface with the upper glass layer and the back cell surface with the rear Tedlar layer. $R_{back,sky}$ and $R_{back,ground}$ are the equivalent resistances due to radiative heat transfer from the Tedlar's rear surface to ground and sky.

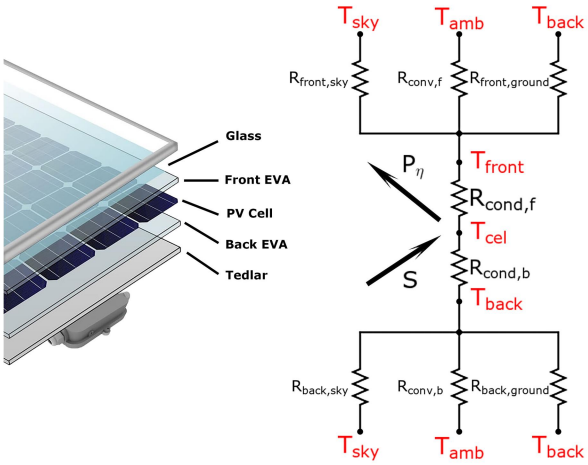

Figure 2. Photovoltaic module layers and equivalent thermal circuit.

The module is schematized in Figure 3 and it is composed by five layers, a frontal layer of glass, an upper EVA layer, a layer of photovoltaic cells, a lower EVA layer and a Tedlar layer. Each layer of each material has a thickness of L_{mat} (in mm), where the subscript *mat* indicates which material is being considered. The finite difference method consists in approximating continuous functions to a series of nodal points in a mesh, converting a differential equation into an algebraic equations system (Özişik, 2017; Incropera *et al*., 2017). The unidimensional heat transfer occurs in the *y* direction and is given by Eq. (7).

$$\rho_i c_i \frac{\partial}{\partial t} T(y,t) = k_i \frac{\partial^2}{\partial y^2} T(y,t) + \dot{Q} \text{ in } L_G \leq y \leq L_T + L_{E_{sup}} + L_{PV} + L_{E_{inf}} + L_T, \text{ for } t > 0 \quad (7)$$

where ρ_i (in kg/m³), c_i (in J/kg.K) and k_i (in W/m.K) represent, respectively, the specific mass, the specific heat and thermal conductivity of each material that composes the photovoltaic module. The parameter $\dot{Q}$ (in W/m³) indicates the internal heat generator inside the glass and photovoltaic cell layers.

The radiative heat transfer coefficients on the top and bottom of the module are given by $h_{r,sup-sink}$, where the subscript *sup* indicates which surface is being considered and *sink* indicates which heat sink is being considered, in this case, either sky or ground, all of them in W/m².K. The coefficients related to the convection heat transfer are represented by h_s for the exchange in the upper module's surface and h_i to the lower module's surface, both in W/m².K.

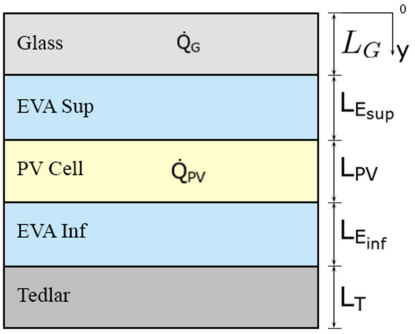

Figure 3. Photovoltaic module layers.

The finite difference method (Özişik, 2017) was employed to solve the differential equations associated with each layer of the studied photovoltaic module. The domain was discretized in a finite number of nodal points. An implicit formulation was used to determine the evolution of the nodal temperatures over time. The thermal contact between each layer of the photovoltaic module was assumed to be perfect.

The glass layer is divided in m_G nodes, $1 \leq m_G \leq N_G$, where N_G is the total number of nodes in the glass. The upper EVA layer is divided into $m_{E_{sup}}$ nodes, $N_G \leq m_{E_{sup}} \leq N_G + N_{E_{sup}} - 1$, where $N_{E_{sup}}$ is the total number of nodes in the upper EVA layer. The photovoltaic cell layer is divided into m_{PV} nodes, $N_G + N_{E_{sup}} - 1 \leq m_{PV} \leq N_G + N_{E_{sup}} + N_{PV} - 2$, where N_{PV} is the total number of nodes in the cell layer. The lower EVA layer is divided into $m_{E_{inf}}$ nodes, $N_G + N_{E_{sup}} + N_{PV} - 2 \leq m_{E_{inf}} \leq N_G + N_{E_{sup}} + N_{PV} + N_{E_{inf}} - 3$, where $N_{E_{inf}}$ is the total number of nodes in the lower EVA layer. The Tedlar layer is divided into m_T nodes, $N_G + N_{E_{sup}} + N_{PV} + N_{E_{inf}} - 2 \leq m_T \leq N_G + N_{E_{sup}} + N_{PV} + N_{E_{inf}} + N_T - 4$, where N_T is the total number of nodes in the Tedlar layer. Equations 8 to 18 represent the discretization of nodal points within the photovoltaic module.

$$\left[\frac{\rho_G c_G \Delta y_G}{2\Delta t}\right]\left(T_{m_G}^{p+1} - T_{m_G}^{p}\right) = \frac{k_G}{\Delta y_G}\left(T_{m_G+1}^{p+1} - T_{m_G}^{p+1}\right) + \dot{Q}_G \frac{\Delta y_G}{2} + h_s\left(T_\infty - T_{m_G}^{p+1}\right) + h_{r,glass,sky}\left(T_{sky} - T_{m_G}^{p+1}\right) + h_{r,glass,ground}\left(T_{ground} - T_{m_G}^{p+1}\right) \text{ for } m_G = 1, \text{ top surface of the glass} \quad (8)$$

$$\left[\frac{\rho_G c_G \Delta y_G}{2\Delta t}\right]\left(T_{m_G}^{p+1} - T_{m_G}^{p}\right) = \frac{k_G}{\Delta y_G}\left(T_{m_G+1}^{p+1} - T_{m_G}^{p+1}\right) + \frac{k_G}{\Delta y_G}\left(T_{m_G-1}^{p+1} - T_{m_G}^{p+1}\right) + \dot{Q}_G \Delta y_G \text{ for } 2 \leq m_G < N_G, \text{ inside of the glass} \quad (9)$$

$$\left[\frac{\rho_G c_G \Delta y_G}{2\Delta t} + \frac{\rho_{E_{sup}} c_{E_{sup}} \Delta y_{E_{sup}}}{2\Delta t}\right]\left(T_{m_{E_{sup}}}^{p+1} - T_{m_{E_{sup}}}^{p}\right) = \frac{k_{E_{sup}}}{\Delta y_{E_{sup}}}\left(T_{m_{E_{sup}}+1}^{p+1} - T_{m_{E_{sup}}}^{p+1}\right) + \frac{k_G}{\Delta y_G}\left(T_{m_{E_{sup}}-1}^{p+1} - T_{m_{E_{sup}}}^{p+1}\right) + \dot{Q}_G \frac{\Delta y_G}{2} \text{ for } m_G = N_G, \text{ interface between the glass and the upper EVA layer} \quad (10)$$

$$\left[\frac{\rho_{E_{sup}} c_{E_{sup}} \Delta y_{E_{sup}}}{\Delta t}\right]\left(T_{m_{E_{sup}}}^{p+1} - T_{m_{E_{sup}}}^{p}\right) = \frac{k_{E_{sup}}}{\Delta y_{E_{sup}}}\left(T_{m_{E_{sup}}-1}^{p+1} - T_{m_{E_{sup}}}^{p+1}\right) + \frac{k_{E_{sup}}}{\Delta y_{E_{sup}}}\left(T_{m_{E_{sup}}+1}^{p+1} - T_{m_{E_{sup}}}^{p+1}\right) \text{ for } N_G < m_{E_{sup}} < N_G + N_{E_{sup}} - 1, \text{ inside of the upper EVA} \quad (11)$$

$$\left[\frac{\rho_{E_{sup}} c_{E_{sup}} \Delta y_{E_{sup}}}{2\Delta t} + \frac{\rho_{PV} c_{PV} \Delta_{yPV}}{2\Delta t}\right]\left(T_{m_{PV}}^{p+1} - T_{m_{PV}}^{p}\right) = \frac{k_{PV}}{\Delta y_{PV}}\left(T_{m_{PV+1}}^{p+1} - T_{m_{PV}}^{p+1}\right) + \frac{k_{E_{sup}}}{\Delta y_{E_{sup}}}\left(T_{m_{PV-1}}^{p+1} - T_{m_{PV}}^{p+1}\right) + \quad (12)$$

$\frac{\dot{Q}_{PV}\Delta y_{PV}}{2}$ for $m_{PV} = N_G + N_{E_{sup}} - 1$, interface between the upper EVA and the photovoltaic cell

$$\left[\frac{\rho_{PV} c_{PV} \Delta y_{PV}}{\Delta t}\right]\left(T_{m_{PV}}^{p+1} - T_{m_{PV}}^{p}\right) = \frac{k_{PV}}{\Delta y_{PV}}\left(T_{m_{PV-1}}^{p+1} - T_{m_{PV}}^{p+1}\right) + \frac{k_{PV}}{\Delta y_{PV}}\left(T_{m_{PV-1}}^{p+1} - T_{m_{PV}}^{p+1}\right) + \dot{Q}_{PV}\Delta y_{PV} \quad \text{for} \quad N_G + N_{E_{sup}} - 1 < m_{PV} < N_G + N_{E_{sup}} + N_{PV} - 2, \text{ inside of the photovoltaic cell} \tag{13}$$

$$\left[\frac{\rho_G c_G \Delta y_G}{2\Delta t} + \frac{\rho_{E_{inf}} c_{E_{inf}} \Delta y_{E_{inf}}}{2\Delta t}\right]\left(T_{m_{E_{inf}}}^{p+1} - T_{m_{E_{inf}}}^{p+1}\right) = \frac{k_{E_{inf}}}{\Delta y_{E_{inf}}}\left(T_{m_{E_{inf}}+1}^{p+1} - T_{m_{E_{inf}}}^{p+1}\right) + \frac{k_G}{\Delta y_G}\left(T_{m_{E_{inf}-1}}^{p+1} - T_{m_{E_{inf}}}^{p+1}\right) + \dot{Q}_G \frac{\Delta y_G}{2} \quad \text{for } m_{PV} = N_G + N_{E_{sup}} + N_{PV} - 2, \text{ interface between the photovoltaic cell and the lower EVA layer} \tag{14}$$

$$\left[\frac{\rho_{E_{inf}} c_{E_{inf}} \Delta y_{E_{inf}}}{\Delta t}\right]\left(T_{m_{E_{inf}}}^{p+1} - T_{m_{E_{inf}}}^{p}\right) = \frac{k_{E_{inf}}}{\Delta y_{E_{inf}}}\left(T_{m_{E_{inf}-1}}^{p+1} - T_{m_{E_{inf}}}^{p+1}\right) + \frac{k_{E_{inf}}}{\Delta y_{E_{inf}}}\left(T_{m_{E_{inf}+1}}^{p+1} - T_{m_{E_{inf}}}^{p+1}\right) \quad \text{for } N_G + N_{E_{sup}} + N_{PV} - 2 < m_{E_{inf}} < N_G + N_{E_{sup}} + N_{PV} + N_{E_{inf}} - 3, \text{ inside of the lower EVA layer} \tag{15}$$

$$\left[\frac{\rho_{E_{inf}} c_{E_{inf}} \Delta y_{E_{inf}}}{2\Delta t} + \frac{\rho_T c_T \Delta_T}{2\Delta t}\right]\left(T_{m_{E_{inf}}}^{p+1} - T_{m_{E_{inf}}}^{p}\right) = \frac{k_T}{\Delta y_T}\left(T_{m_{E_{inf}}+1}^{p+1} - T_{m_{E_{inf}}}^{p+1}\right) + \frac{k_{E_{sup}}}{\Delta y_{E_{sup}}}\left(T_{m_{PV-1}}^{p+1} - T_{m_{E_{inf}}}^{p+1}\right) + \frac{\dot{Q}_{PV}\Delta y_{PV}}{2} \quad \text{for } m_{E_{inf}} = N_G + N_{E_{sup}} + N_{PV} + N_{E_{inf}} - 3, \text{ interface between the lower EVA layer and the Tedlar layer} \tag{16}$$

$$\left[\frac{\rho_T c_T \Delta y_T}{2\Delta t}\right]\left(T_{m_T}^{p+1} - T_{m_T}^{p}\right) = \frac{k_T}{\Delta y_T}\left(T_{m_T+1}^{p+1} - T_{m_T}^{p+1}\right) + \frac{k_T}{\Delta y_T}\left(T_{m_T-1}^{p+1} - T_{m_T}^{p+1}\right) \quad \text{for} \quad N_G + N_{E_{sup}} + N_{PV} + N_{E_{inf}} - 3 < m_T < N_G + N_{E_{sup}} + N_{PV} + N_{E_{inf}} + N_T - 4, \text{ inside the Tedlar layer} \tag{17}$$

$$\left[\frac{\rho_T c_T \Delta y_T}{2\Delta t}\right]\left(T_{m_T}^{p+1} - T_{m_T}^{p}\right) = \frac{k_T}{\Delta y_T}\left(T_{m_T-1}^{p+1} - T_{m_T}^{p+1}\right) + h_i\left(T_\infty - T_{m_T}^{p+1}\right) + h_{r,tedlar-sky}\left(T_{sky} - T_{m_T}^{p+1}\right) + h_{r,tedlar-ground}\left(T_{ground} - T_{m_T}^{p+1}\right) \text{ for } m_T = N_G + N_{E_{suo}} + N_{PV} + N_{E_{inf}} + N_T - 4, \text{ bottom Tedlar surface} \tag{18}$$

where Δy_{mat} is the distance between each node according to the selected material and Δt indicates the time step.

2.4 Coupling of the Thermal and Electrical Models

The first step in the coupled solution of the thermal-electric model is to input the program with the climatological data of the location, as well as the physical (electrical and thermal) and geometric properties of the photovoltaic module. Then, the electrical model is executed for the first time to obtain the initial value of the electrical efficiency of the photovoltaic module, denoted as η_{ini}. To calculate η_{ini}, an initial average temperature is assigned to the photovoltaic cell ($T_{cel,ini}$). Next, the steady-state thermal calculations are performed, resulting in a temperature field based on the previously calculated efficiency value. From this field, an average value for T_{cel} is extracted, and the values of T_{cel} and $T_{cel,ini}$ are compared. The absolute difference between them is compared to a predefined tolerance value. If this difference is greater than or equal to the tolerance, $T_{cel,ini}$ becomes equal to T_{cel}, and the program returns to calculate η with the new temperature values. When the difference is less than the specified tolerance, the program determines a final value for T_{cel}. Once a temperature field is determined for the steady-state model, the transient model is executed, following the same logical principle, with the additional inclusion of a loop for each time step interval of Δt = 30 seconds between sunrise and sunset for each simulated day. The process described above is further detailed in the following steps:

Step 1. Input the initial program data: climatological data of the location, along with the physical (electrical and thermal) and geometric properties of the photovoltaic module.
Step 2. Compute the initial temperature field ($T_{cel,ini}$).
Step 3. Calculate the properties of the air using the temperature field.
Step 4. Use the initial values of $T_{cel,ini}$ and G_i in the electrical model, generating an output η.
Step 5. Use the values of η, climatological data, geometric data, and air properties in the steady-state model, generating the cell temperature T_{cel}.
Step 6. If $\left|T_{cel,ini} - T_{cel}\right| > tol$, define $T_{cel,ini} = T_{cel}$ and repeat steps 2 to 5.
Step 7. After determining the initial temperature field of the steady-state model, set the time step for the start of the transient solution.
Step 8. Calculate the properties of the air using the initial temperature field.

Step 9. Use values of $T_{cel,ini}$ and G_i from the current time step in the electrical model, generating an output η.
Step 10. Use the values of η, climatological data, geometrical data and air properties in the transient model, generating the cell temperature T_{cel}.
Step 11. If $|T_{cel,ini} - T_{cel}| > tol$, define $T_{cel,ini} = T_{cel}$ and repeat steps 7 to 10.
Step 12. If $|T_{cel,ini} - T_{cel}| < tol$, increment the time step.
Step 13. If current time step < final time step, repeat steps 7 to 12.

where tol is the tolerance value (in this case, $tol \approx$ 10e-7).

3. RESULTS AND DISCUSSION

In this work, the modelled photovoltaic module is the ND-220E1F, from Sharp. The thermophysical and geometrical parameters of the photovoltaic module were adapted from the datasheet of the module's manufacturer and from Armstrong and Hurley (2010) and are presented in Table 1.

Table 1. Photovoltaic module properties.

MATERIAL	THICKNESS (m)	THERMAL CONDUCTIVITY (W/m.K)	DENSITY (kg/m³)	SPECIFIC HEAT CAPACITY (J/kg.C)
Glass	0,003	1,8	3000	500
EVA	150×10^{-6}	0,35	690	2090
PV Cells	225×10^{-6}	148	2330	677
Tedlar	100×10^{-6}	0,2	1200	1250

The calculated values with the thermal-electrical model of this paper are represented in the following graphs as *TE Author*, for the arithmetic mean of the temperatures of the nodes inside the photovoltaic cells, T_{cel}, and for the electrical efficiency of the photovoltaic module, η. The graphs were plotted as a function of the standard time of day - from sunrise to sunset, in 30 seconds intervals for each average day. The results were compared with other five models found in literature, three of them being fully thermal *T Ross & Smokler, T Mondol, T Risser & Fuentes* (Ross (1976), Mondol *et al.* (2005), Risser and Fuentes (1983)) and two thermal-electrical models *TE Duffie* e *TE King* (Duffie *et al.* (2013) and King *et al.* (2004)).

The evolution of the photovoltaic cell temperatures and efficiency during the average day of each selected month are represented in Figures 4 to 7. Those average days are the ones that represent the summer and winter solstices months, June 11 (T_∞= 25,61 °C, V_w = 4,44 m/s) and December 10 (T_∞ = 27,07 °C, V_w = 4,30 m/s), as well as the equinox months March 16 (T_∞ = 27,45 °C, V_w = 3.69 m/s) and September 15 (T_∞ = 25.09 °C, V_w = 4,66 m/s), in the southern hemisphere.

The efficiency graphs of the photovoltaic module calculated by each model, shown in Figure 4b to 7b, presented different values for each average day, however, the shape of the model curves remained constant for all simulated days. Similarly, the photovoltaic cell temperatures also present similar behaviors for each used model, shown in Figure 4a to 7a.

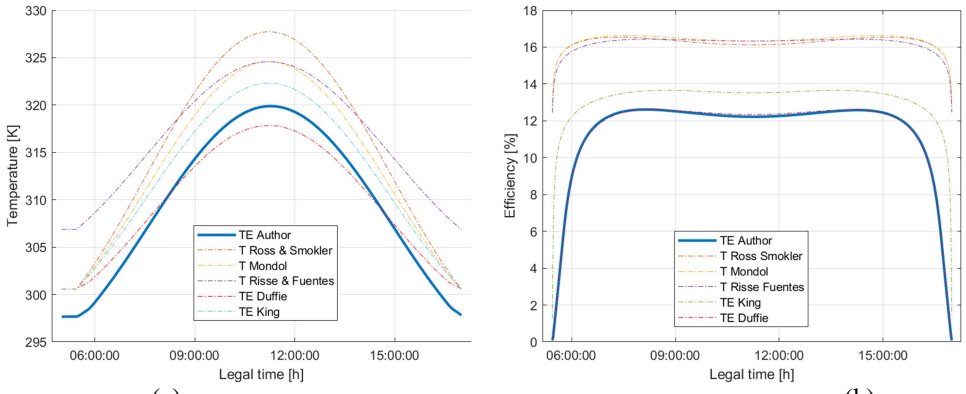

(a) (b)

Figure 4. Comparison graphs (a) of photovoltaic cell temperature and (b) of photovoltaic module efficiency throughout the simulated day of 16/03, between the developed thermal-electric model (*TE Author*) and other models.

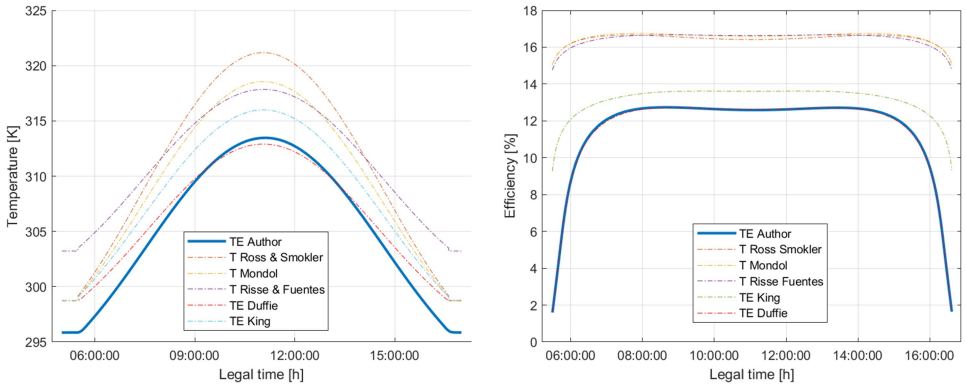

(a) (b)

Figure 5. Comparison graphs (a) of photovoltaic cell temperature and (b) of photovoltaic module efficiency throughout the simulated day of 11/06, between the developed thermal-electric model (*TE Author*) and other models.

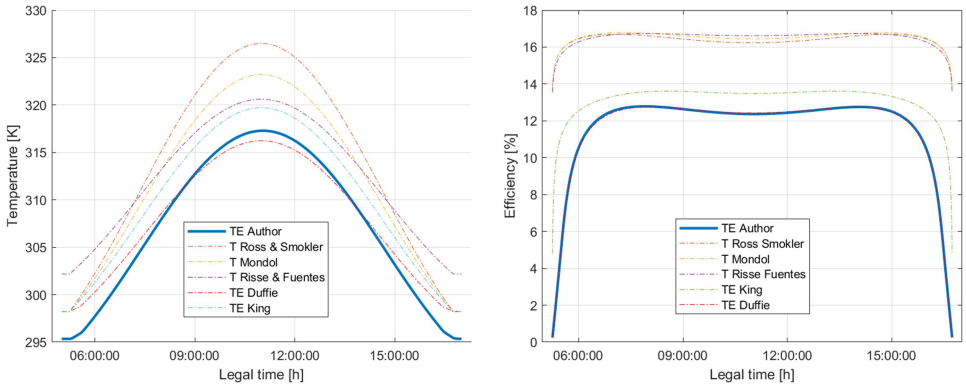

(a) (b)

Figure 6. Comparison graphs (a) of photovoltaic cell temperature and (b) of photovoltaic module efficiency throughout the simulated day of 15/09, between the developed thermal-electric model (*TE Author*) and other models.

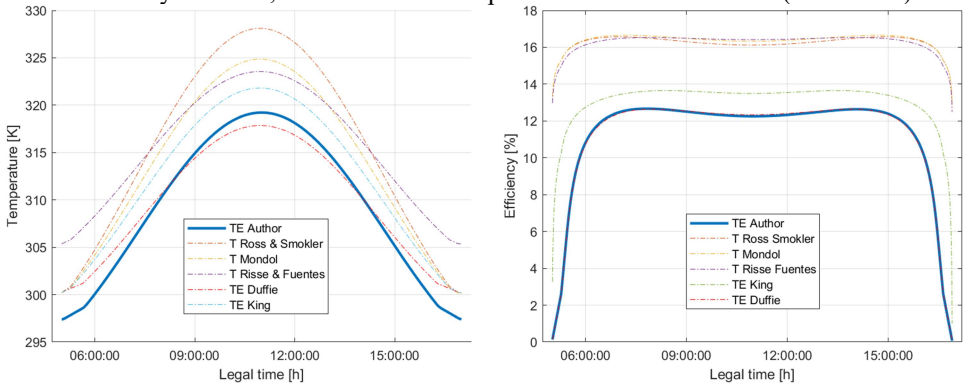

(a) (b)

Figure 7. Comparison graphs (a) of photovoltaic cell temperature and (b) of photovoltaic module efficiency throughout the simulated day of 11/12, between the developed thermal-electric model (*TE Author*) and other models.

Among the four selected average days for study in this work, the average day of March (16/03) was the one that presented higher values of photovoltaic cell temperatures (T_{cel}) calculated by the analyzed thermal-electric models, shown in Figure 4a; for solar noon, at the local time of 11:48 a.m. The occurrence of these higher temperatures in the photovoltaic cell is likely caused by the combination of higher average air temperature (T_{∞}), lower average wind speed, and an important solar irradiation value for the simulated month. Furthermore, among the four average days, 16/03 corresponds to the day when the apparent trajectory of the Sun in the sky is closest to the latitude where the module is located, that is, the latitude of the site (ϕ = -7.14°) is relatively close to the solar declination of 16/03 (δ = -2.31°). This favors the capture of solar energy by the module but contributes to its heating.

The average day of June (11/06) was the one that presented the lowest values of T_{cel}, in Figure 5a, among all the analyzed days. This occurs due to the weak tilt of the photovoltaic module, associated with the fact that on the 16th of June, the apparent trajectory of the Sun in the sky is far from the latitude where the module is located, meaning that the latitude of the location is very different from the solar declination on that day (δ = +23.08°).

In the months of June and September, all models showed the highest electrical efficiencies of the photovoltaic module. However, the efficiencies of the purely thermal models studied in this work used generic correlations for calculating η instead of employing an appropriate electrical model. As a result, the efficiency becomes predominantly dependent on the cell temperature variation, disregarding the proper changes caused by variations in G_i values, leading to an overestimation of η values, which can be higher than the efficiency values reported in the datasheet of the studied photovoltaic module.

The *TE Author*, *TE Duffie*, and *TE King* models showed the maximum efficiency values among the four analyzed average days on the 15th of September, shown in Figure 5b. This occurred because this day was characterized by an important solar radiation incidence, associated with high wind speed and low air temperature. It was observed that the cell temperatures calculated by these three models were lower than those calculated by the same models on the average day of 15/09, shown in Figure 6a.

According to Figure 7a, for the average day of December (11/12), the purely thermal models showed high values of T_{cel} for solar noon (legal time of 11h46) when compared to the corresponding values of the average days 15/09 and 11/06, as observed in Figure 6a and Figure 5a, respectively. It is observed that the T_{cel} values are relatively close to those in Figure 4a. This occurs because, despite the apparent trajectory of the Sun being far from the module's latitude (δ = -23.12°), the solar irradiation is the highest among the analyzed months due to the proximity to the summer solstice date.

Table 2 presents the daily averages of the arithmetic mean photovoltaic cells temperatures. ($T_{cel,med}$, in K) of each analyzed model for each average simulated day. The penultimate column of this table presents the arithmetic mean of each model's $T_{cel,med}$, for the four simulated days ($\overline{T}_{cel,med}$, in K). The last column presents the difference ($\Delta\overline{T}_{cel,med}$, in K) between $\overline{T}_{cel,med}$ of the models *TE King*, *TE Duffie*, *T Ross & Smokler*, *T Mondol* e *T Risser & Fuentes* in relation to the model *TE Author*. For the four average days, the models that presented the closest $\overline{T}_{cel,med}$ to the one developed in this work were *TE Duffie* ($\Delta\overline{T}_{cel,med} = 0{,}50$ K) and *TE King* ($\Delta\overline{T}_{cel,med} = 2{,}88$ K). On the other hand, the model that presented the highest value of $\overline{T}_{cel,med}$ and most distant to *TE Author* was the model of *T Ross & Smokler*.

Table 2. Mean temperatures of the photovoltaic cell ($T_{cel,med}$), of each analysed model, for each simulated day.

MODELS	DAY	16/03	11/06	15/09	11/12	$\overline{T}_{cel,med}$ (K)	$\Delta\overline{T}_{cel,med}$ (K)
TE Author	$T_{cel,med}$	309,93	305,40	307,39	309,50	308,05	---
TE King		312,77	308,26	310,25	312,45	310,93	2,88
TE Duffie		309,99	306,35	308,00	309,88	308,55	0,50
T Ross & Smokler		315,81	311,11	314,04	316,02	314,24	6,19
T Mondol		314,01	309,64	312,17	314,15	312,50	4,44
T Risser & Fuentes		316,80	311,29	312,49	315,67	314,06	6,01

Table 3. Maximum photovoltaic module efficiency calculated by each model, for each simulated day.

MODELS	DAY	16/03	11/06	15/09	11/12	$\overline{\eta}_{max}$ (%)	$\Delta\overline{\eta}_{max}$ (%)
TE Author	η_{max}	12,61	12,74	12,78	12,67	12,70	---
TE King		13,66	13,62	13,61	13,65	13,64	0,93
TE Duffie		12,61	12,71	12,75	12,64	12,68	-0,02
T Ross & Smokler		16,54	16,66	16,70	16,57	16,62	3,92
T Mondol		16,63	16,75	16,78	16,65	16,70	4,00
T Risser & Fuentes		16,43	16,67	16,74	16,53	16,59	3,89

The electrical efficiency curves of the photovoltaic module, η, calculated by the analyzed models, for each simulated days (Figure 4b to 7b), present similar shapes. All of the models start the day with $\eta = 0$ and reach the maximum efficiency values within the first and last hours of the day. The purely thermal models all present values of efficiency higher than those provided by the datasheet of the photovoltaic module. The thermal-electrical models present more reasonable values for efficiency, because of the G_i parameter higher influence when determining η. For all models, η decreases when nearing solar noon time, which shows the combined influence of T_{cel} and G_i when determining η. For each simulated day, Table 3 shows the maximum values calculated of η by each model on each

simulated day, the average of those values ($\overline{\eta}_{max}$) and the difference between those averages of each model in relation to the efficiency values obtained by TE Author ($\Delta\overline{\eta}_{max}$). The models that presented the closest $\overline{\eta}_{max}$ to the one developed in this work were *TE Duffie* ($\Delta\overline{\eta}_{max} = -0{,}02\ \%$) and *TE King* ($\Delta\overline{\eta}_{max} = 0{,}93\ \%$). On the other hand, the model that presented the highest value of $\overline{\eta}_{max}$ and most distant to *TE Author* was the model of *T Mondol*.

4. CONCLUSION

In this paper a computational model for a photovoltaic module was developed, aiming to obtain realistic data when referring to photovoltaic cell temperature and the module's electrical efficiency. A thermal-electrical model was developed based on a coupled solution of a purely thermal model, based on energy balances of thermal energy on the module (Aly *et al.,* 2017), and a purely electrical model presented by Villalva *et al.* (2009). The expanded thermal-electrical model is advantageous because it computes the thermophysical and geometrical properties of the module with the addition of the module's electrical properties.

The mean photovoltaic cells temperatures calculated by the author's model were relatively close to those calculated with the other five analyzed models (Figure 4a to 7a). That was evident when the mean cell temperatures were compared, showing that the developed model in this paper is adequate do estimate the temperature T_{cel} of photovoltaic modules.

When there is no solar radiation, the photogenerated current I_{pv} equals to 0. This implies that the electrical efficiency of the photovoltaic module is null (Durisch, 2007). In that sense, all the models present reasonable values of efficiency. However, the efficiencies calculated by the thermal-electrical models where always inferior to $\eta_{STC} = 13{,}4\%$, as expected of photovoltaic modules in real operating conditions.

5. REFERENCES

Aly S. P., Ahzi S., Barth N., Figgis B. W., 2018. "Two-dimensional finite difference-based model for coupled irradiation and heat transfer in photovoltaic modules". Solar Energy Materials and Solar Cells, Vol. 180, pp. 289-302.

Armstrong S., Hurley W. G., 2010. "A thermal model for photovoltaic panels under varying atmospheric conditions". Applied Thermal Engineering, v. 30, p. 1488-1495.

Brano V. L., Ciulla G., Piacentino A., Cardona F., 2014 "Finite difference thermal model of a latent heat storage system coupled with a photovoltaic device: Description and experimental validation". Renewable Energy, v. 68, p. 181-193.

Duffie, J. A., Beckman, W. A, Blair N., 2020. Solar Engineering of Thermal Processes, Photovoltaics and Wind. John Wiley & Sons.

Durisch W., Bitnar B., Mayor J. C., Kiess H., Lam K. H., Close J., 2007. "Efficiency model for photovoltaic modules and demonstration of its application to energy yield estimation", Solar Energy Materials & Solar Cells 91 (2007) 79–84.

IEA, 2022. Solar PV. International Energy Agency, iea.org. Accessed 20 April 2023.

Incropera, F. P., Lavine A.S, Bergman T.L., Dewitt D. P., 2017. Fundamentals of Heat and Mass Transfer. John Wiley & Sons.

Jakhrani A. Q., Othman A. K., Rigit A. R. H., Samo S.R., Kamboh S. A., 2013. "Sensitivity Analysis of a Standalone Photovoltaic System Model Parameters". Journal of Applied Sciences, 13: 220-231.

King, D. L., Boyson W.E., Kratochvill J.A., 2004. Photovoltaic Array Performance Model, Sandia Report.

Mondol J. D., Yohanis Y. G., Smyth M., Norton B, 2005. "Long-term validated simulation of a building integrated photovoltaic system". Solar Energy, v. 78, p. 163-176.

Özişik, M.N., Orlande, H.R.B., Colaço, M.J., & Cotta, R.M., 2017. "Finite difference Methods in Heat Transfer", CRC Press. Boca Raton (USA)

Risser, V. V., Fuentes, M. K., 1984. "Linear regression analysis of flat-plate photovoltaic system performance data.", Proceedings of the 5th Photovoltaic Solar Energy Conference.

Ross, R. G., 1976. "Interface design considerations for terrestrial solar cell modules", 12th Photovoltaic Specialists Conferece.

Skoplaki E., Palyvos J. A., 2009. "Operating temperature of photovoltaic modules: A survey of pertinent correlations". Renewable Energy 34.

Tuza, A. O.; Mahieddine, E. A., 2014. "Comparative Analysis of PV Module Temperature Models". Energy Procedia Vol. 62.

Villalva, M. G., Gazoli, J. R., Ruppert Filho, E., 2009. "Modeling and circuit-based simulation of photovoltaic arrays", IEEE Xplore.

6. RESPONSIBILITY NOTICE

The authors are the only responsible for the printed material included in this paper.